



1 **Converting Snow Depth to Snow Water Equivalent Using** 2 **Climatological Variables**

3
4 David F. Hill¹, Elizabeth A. Burakowski², Ryan L. Crumley³, Julia Keon⁴, J. Michelle Hu⁵,
5 Anthony A. Arendt⁶, Katreen Wikstrom Jones⁷, Gabriel J. Wolken⁸

6
7 ¹Civil and Construction Engineering, Oregon State University, OR, USA

8 ²Institute for the Study of Earth, Oceans, and Space, University of New Hampshire, NH, USA

9 ³Water Resources Graduate Program, Oregon State University, OR, USA

10 ⁴Civil and Construction Engineering, Oregon State University, OR, USA

11 ⁵Civil and Environmental Engineering, University of Washington

12 ⁶Applied Physics Laboratory, University of Washington

13 ⁷Alaska Division of Geological & Geophysical Surveys, Fairbanks, AK, USA

14 ⁸Alaska Division of Geological & Geophysical Surveys, Fairbanks, AK, USA; International Arctic Research Center,
15 University of Alaska Fairbanks, Fairbanks, AK, USA

16 *Correspondence to:* David F. Hill (david.hill@oregonstate.edu)

17
18
19 **Abstract.** We present a simple method that allows snow depth measurements to be converted to snow water
20 equivalent (SWE) estimates. These estimates are useful to individuals interested in water resources, ecological
21 function, and avalanche forecasting. They can also be assimilated into models to help improve predictions of total
22 water volumes over large regions. The conversion of depth to SWE is particularly valuable since snow depth
23 measurements are far more numerous than costlier and more complex SWE measurements. Our model regresses
24 SWE against snow depth and climatological (30-year normal) values for mean annual precipitation (*MAP*) and mean
25 February temperature, producing a power-law relationship. Relying on climatological normals rather than weather
26 data for a given year allows our model to be applied at measurement sites lacking a weather station. Separate
27 equations are obtained for the accumulation and the ablation phases of the snowpack, which introduces ‘day of
28 water year’ (DOY) as an additional variable. The model is validated against a large database of snow pillow
29 measurements and yields a bias in SWE of less than 0.5 mm and a root-mean-squared-error (RMSE) in SWE of
30 approximately 65 mm. When the errors are investigated on a station-by-station basis, the average RMSE is about 5%
31 of the *MAP* at each station. The model is additionally validated against a completely independent set of data from
32 the northeast United States. Finally, the results are compared with other models for bulk density that have varying
33 degrees of complexity and that were built in multiple geographic regions. The results show that the model described
34 in this paper has the best performance for the validation data set.



35 **1 Introduction**

36 In many parts of the world, snow plays a leading-order role in the hydrological cycle (Mote et al., 2018). Accurate
37 information about the spatial and temporal distribution of snow water equivalent (SWE) is useful to many
38 stakeholders (water resource planners, avalanche forecasters, aquatic ecologists, etc.), but can be time consuming
39 and expensive to obtain.

40

41 Snow pillows (Beaumont, 1965) are a well-established tool for measuring SWE at fixed locations. Figure 1 provides
42 a conceptual sketch of the variation of SWE with time over a typical water year. A comparatively long accumulation
43 phase is followed by a short ablation phase. While simple in operation, snow pillows are relatively large in size and
44 they need to be installed prior to the onset of the season's snowfall. This limits their ability to be rapidly or
45 opportunistically deployed. Additionally, snow pillow installations tend to require vehicular access, limiting their
46 locations to relatively simple topography, and are not representative of the lowest or highest elevation bands within
47 mountainous regions (Molotch and Bales, 2005). In the western United States (USA), the Natural Resources
48 Conservation Service (NRCS) operates a large network of Snow Telemetry (SNOTEL) sites, featuring snow
49 pillows. The NRCS also operates the smaller Soil Climate Analysis Network (SCAN) which provides the only, and
50 very limited, snow pillow SWE measurements in the eastern USA.

51

52 SWE can also be measured manually, using a snow coring device that measures the weight of a known volume of
53 snow to determine snow density (Church, 1933). These measurements are often one-off measurements, or in the
54 case of 'snow courses' they are repeated weekly or monthly at a given location. The simplicity and portability of
55 these devices expand the range over which measurements can be collected, but it can be challenging to apply these
56 methods to deep snowpacks due to the length of standard coring devices and/or the need to dig very deep snowpits.
57 Studies comparing different styles of snow samplers report statistically different results, suggesting that SWE
58 measurements are sensitive to the design of the coring device, such as the presence of holes or slots, the device
59 material, etc. (Beaumont and Work, 1963; Dixon and Boon, 2012).

60

61 Finally, SWE can be estimated with remote sensing methods, including satellite, airborne, and fixed platforms (e.g.,
62 Sokol et al., 2003; Vuyovich et al., 2014). Microwave frequencies are commonly used, but these frequencies do not
63 work well in the presence of liquid water in the snowpack (Leinss et al., 2015). Recent attention has focused on the
64 superior ability of L-band frequencies to measure SWE in wet snowpacks. Kang and Barros (2011) developed and
65 tested an L-band snow sensor system in laboratory conditions and Deeb et al. (2017) discuss the application of L-
66 band measurements to field-scale snow depth and SWE estimates for the SnowEx project.

67

68 All methods of measuring SWE are challenged by the fact that SWE is a depth-integrated property of a snowpack.
69 This is why the snowpack must be weighed, in the case of a snow pillow, or a core must be extracted from the
70 surface to the ground. This measurement complexity makes it difficult to obtain SWE information with the spatial
71 and temporal resolution desired for watershed-scale studies. Other snowpack properties, such as the depth h , are



72 much easier to measure. Using a graduated device such as a meterstick or an avalanche probe to measure the depth
73 takes only seconds, and depth measurements at a fixed location are easily automated using low-cost ultrasonic
74 devices (Ryan et al., 2008). High-spatial-resolution measurements of snowpack depth are commonly made with
75 Light Detection and Ranging (LIDAR). One example of this is the Airborne Snow Observatory program (ASO;
76 Painter et al., 2016). The comparatively high expense of airborne LIDAR surveys typical limits measurements
77 geographically (to a few basins) and temporally (weekly to monthly interval).

78
79 Given the relative ease in obtaining depth measurements, it is common to use h as a proxy for SWE. Figure 1 shows
80 a conceptual sketch of the variation of SWE with h over a typical water year. Noting the arrows on the curve, we see
81 that SWE is multi-valued for each h . This is due to the fact that the snowpack increases in density throughout the
82 water year, producing a hysteresis loop in the curve. A large body of literature exists on the topic of how to convert
83 h to SWE. It is beyond the scope of this paper to provide a full review of these ‘bulk density equations,’ where the
84 density is given by $\rho_b = SWE/h$. Instead, we refer readers to the useful comparative review by Avanzi et al. (2015).
85 Here, we prefer to discuss a limited number of previous studies that illustrate the spectrum of methodologies and
86 complexities that can be used to determine ρ_b or SWE.

87
88 Many studies express ρ_b as an increasing function (often linear) of h . In some cases (e.g., Lundberg et al., 2006) a
89 second equation is added where ρ_b attains a constant value when a threshold h is exceeded. A single linear equation
90 captures the process of densification of the snowpack during the accumulation phase, but performs poorly during the
91 ablation phase, where depths are decreasing but densities continue to increase or approach a constant value.
92 Other approaches choose to parameterize ρ_b in terms of time, rather than h . Pistocchi (2016) provides a single
93 equation while Mizukami and Perica (2008) provide two sets of equations, one set each for early and late season.
94 Each set contains four equations, each of which is applicable to a particular ‘cluster’ of stations. This clustering was
95 driven by observed densification characteristics and the resulting clusters are relatively spatially discontinuous.
96 Jonas and Magnusson (2009) take the idea of region- (or cluster-) specific equations and extend it further to provide
97 coefficients that depend on time and elevation as well. They use a simple linear equation for ρ_b in terms of h and the
98 slope and intercept of the equation are given as monthly values, with three elevation bins for each month (36 pairs of
99 coefficients). There is an additional contribution to the intercept (or ‘offset’) which is region-specific (one of 7
100 regions).

101
102 These classifications, whether based on region, elevation, or season, are valuable since they acknowledge that all
103 snow is not equal. Sturm et al. (2010) address this directly by developing a snow density equation where the
104 coefficients depend upon the ‘snow class’ (5 classes). Sturm et al. (1995) explain the decision tree, based on
105 temperature, precipitation, and wind speed, that leads to the classification. The temperature metric is the ‘cooling
106 degree month’ calculated during winter months only. Similarly, only precipitation falling during winter months was
107 used in the classification. Finally, given the challenges in obtaining high quality, high-spatial-resolution wind



108 information, vegetation classification was used as a proxy. Using climatological values (rather than values for a
109 given year), Sturm et al. (1995) were able to develop a global map of snow classification.

110
111 There are many other formulations for snow density that increase in complexity and data requirements. Meloyund
112 et al. (2007) express ρ_b in terms of sub-daily measurements of relative humidity, wind characteristics, air pressure,
113 and rainfall, as well as h and estimates of solar exposure ('sun hours'). McCreight and Small (2014) use daily snow
114 depth measurements to develop their regression equation. They demonstrate improved performance over both Sturm
115 et al. (2010) and Jonas and Magnusson (2009). However, a key difference between the McCreight and Small (2014)
116 model and the others listed above is that the former cannot be applied to a single snow depth measurement. Instead,
117 it requires a continuous time series of depth measurements at a fixed location. Further increases in complexity (and
118 correspondingly, accuracy) are found in energy-balance snowpack models (SnowModel, Liston and Elder, 2006;
119 VIC, Liang et al., 1994, DHSVM, Wigmosta et al., 1994, others). While the particular details vary, these models
120 generally require high temporal-resolution time series of many meteorological variables as input. Also, many of
121 these models resolve vertical variations in snow density which are wholly absent from the bulk (vertically averaged)
122 density approaches reviewed above.

123
124 Despite the development of multi-layer energy-balance snow models, there is still a demonstrated need for bulk
125 density formulations and for vertically integrated data products like SWE. Pagano et al. (2009) review the
126 advantages and disadvantages of energy-balance models and statistical models and describe how the NRCS uses
127 SWE (from SNOTEL stations) and accumulated precipitation in their statistical models to make daily water supply
128 forecasts. If SWE information is desired at a location that does not have a SNOTEL station, and if not part of a
129 modeling effort, then bulk density equations and depth measurements are an excellent choice.

130
131 The present paper seeks to generalize the ideas of Mizukami and Perica (2008), Jonas and Magnusson (2009), and
132 Sturm et al., (2010). Specifically, our goal is to regress physical and environmental variables directly into the
133 equations. In this way, environmental variability is handled in a continuous fashion rather than in a discrete way
134 (model coefficients based on classes). The main motivation for this comes from evidence (e.g., Fig. 3 of Alford,
135 1967) that density can vary significantly over short distances on a given day. Bulk density equations that rely solely
136 on time completely miss this variability and equations that have coarse (model coefficients varying over either
137 vertical bins or horizontal grids) spatial resolution may not fully capture it either.

138
139 Our approach is most similar to Mizukami and Perica (2008), Jonas and Magnusson (2009), and Sturm et al., (2010)
140 in that a minimum of information is needed for the calculations; we intentionally avoid approaches like Meloyund
141 et al. (2007) and McCreight and Small (2014). This is because our interests are in converting h measurements to
142 SWE estimates in areas lacking weather instrumentation. The following sections introduce the numerous data sets
143 that were used in this study, outline the regression model adopted, and assess the performance of the model.



144 **2 Methods**

145

146 **2.1 Data**

147

148 **2.1.1 Snow Depth and Snow Water Equivalent**

149 In this section, we list sources of 1970-present snow data utilized for this study (Table 1).

150

151 **2.1.1.1 USA NRCS Snow Telemetry and Soil Climate Analysis Networks**

152 SNOTEL (Serreze et al., 1999; Dressler et al., 2006) and SCAN (Schaefer et al. 2007) stations in the contiguous
153 United States (CONUS) and Alaska typically record sub-daily observations of h , SWE, and a variety of weather
154 variables (Figure 2a-b). The periods of record are variable, but the vast majority of stations have a period of record
155 in excess of 30 years. For this study, data from all SNOTEL sites in CONUS and Alaska and northeast USA SCAN
156 sites were obtained with the exception of sites whose period of record data were unavailable online. Only stations
157 with both SWE and h data were retained.

158

159 **2.1.1.2 Canada (British Columbia) Snow Survey Data**

160 Goodison et al. (1987) note that Canada has no national digital archive of snow observations from the many
161 independent agencies that collect snow data and that snow data are instead managed provincially. The quantity and
162 availability of the data vary considerably among the provinces. The Water Management Branch of the British
163 Columbia (BC) Ministry of the Environment manages a comparatively dense network of Automated Snow Weather
164 Stations (ASWS) that measure SWE, h , accumulated precipitation, and other weather variables (Figure 2a). For this
165 study, data from all British Columbia ASWS sites were initially obtained. As with the NRCS stations, only ASWS
166 stations with both SWE and h data were retained.

167

168 **2.1.1.3 Northeast USA Data**

169 Snow data for this project from the northeast US come from two networks and three research sites (Figure 2b). The
170 Maine Cooperative Snow Survey (MCSS, 2018) network includes h and SWE data collected by the Maine
171 Geological Survey, the United States Geological Survey, and numerous private contributors and contractors. MCSS
172 snow data are collected using the Standard Federal or Adirondack snow sampling tubes typically on a weekly to bi-
173 weekly schedule throughout the winter and spring, 1951-present. The New York Snow Survey network data were
174 obtained from the National Oceanic and Atmospheric Administration's Northeast Regional Climate Center at
175 Cornell University (NYSS, 2018). Similar to the MCSS, NYSS data are collected using Standard Federal or
176 Adirondack snow sampling tubes on weekly to bi-weekly schedules, 1938-present.

177

178 The Sleepers River, Vermont Research Watershed in Danville, Vermont (Shanley and Chalmers, 1999) is a USGS
179 site that includes 15 stations with long-term weekly records of h and SWE collected using Adirondack snow tubes.
180 Most of the periods of record are 1981-present, with a few stations going back to the 1960s. The sites include



181 topographically flat openings in conifer stands, old fields with shrub and grass, a hayfield, a pasture, and openings in
182 mixed softwood-hardwood forests. The Hubbard Brook Experiment Forest (Campbell et al., 2010) has collected
183 weekly snow observations at the Station 2 rain gauge site, 1959-present. Measurement protocol collects ten samples
184 2 m apart along a 20 m transect in a hardwood forest opening about $\frac{1}{4}$ hectare in size. At each sample location along
185 the transect, h and SWE are measured using a Mt. Rose snow tube and the ten samples are averaged for each
186 transect. Finally, the Thompson Farm Research site includes a mixed hardwood forest site and an open pasture site
187 (Burakowski et al. 2013; Burakowski et al. 2015). Daily (from 2011-2018), at each site, a snow core is extracted
188 with an aluminum tube and weighed (tube + snow) using a digital hanging scale. The net weight of the snow is
189 combined with the depth and the tube diameter to determine ρ_b , similar to a Federal or Adirondack sampler.

190

191 **2.1.1.4 Chugach Mountains (Alaska) Data**

192 In the spring of 2018, we conducted three weeks of fieldwork in the Chugach mountains in coastal Alaska, near the
193 city of Valdez (Figure 2c-d). We measured SWE using a Federal sampler at 71 sites along elevational transects
194 during March, April, and May. The elevational transects ranged between 250 and 1100 m (net change along
195 transect) and were accessible by ski and snowshoe travel. At each of those 71 sites, we took 3 SWE and h
196 measurements within 1 m² and averaged the result. Additionally, we used an avalanche probe to measure h in 8
197 locations within the surrounding 10 m², resulting in a total of 550+ snow depth measurements. These 71 sites were
198 scattered across 8 regions in order to capture spatial gradients in snow densities that exist in the Chugach mountains
199 as the wetter, more-dense maritime snow near the coast gradually changes to drier, less dense snow on the interior
200 side.

201

202 **2.1.1.5 Outlier Detection and Removal**

203 Figure 3 demonstrates that it is not uncommon for automated snow depth measurements to become noisy or non-
204 physical, at times reporting large depths when there is no SWE reported. It was therefore desirable to apply some
205 objective, uniform procedure to each station's dataset in order to remove clear outlier points. We recognize that
206 there is no accepted standardized method for cleaning bivariate SWE- h data sets. While Serreze et al. (1999) offer a
207 procedure for SNOTEL data in their appendix, it is relevant only for precipitation and SWE values, not h . Given the
208 strong correlation between h and SWE, we instead choose to use common outlier detection techniques for bivariate
209 data.

210

211 The Mahalanobis distance (MD; Maesschalck et al., 2000) quantifies how far a point lies from the mean of a
212 bivariate distribution. The distances are in terms of the number of standard deviations along the respective principal
213 component axes of the distribution. For highly correlated bivariate data, the MD can be qualitatively thought of as a
214 measure of how far a given point deviates from an ellipse enclosing the bulk of the data. One problem is that the MD
215 is based on the statistical properties of the bivariate data (mean, covariance) and these properties can be adversely
216 affected by outlier values. Therefore, it has been suggested (e.g., Leys et al., 2018) that a 'robust' MD (RMD) be
217 calculated. The RMD is essentially the MD calculated based on statistical properties of the distribution unaffected



218 by the outliers. This can be done using the Minimum Covariance Determinant (MCD) method as first introduced by
 219 Rousseeuw (1984).

220
 221 Once RMDs have been calculated for a bivariate data set, there is the question of how large an RMD must be in
 222 order for the data point to be considered an outlier. For bivariate normal data, the distribution of the square of the
 223 RMD is χ^2 (Gnanadesikan and Kettenring, 1972), with p (the dimension of the dataset) degrees of freedom. So, a
 224 rule for identifying outliers could be implemented by selecting as a threshold some arbitrary quantile (say 0.99) of
 225 χ_p^2 . For the current study, a threshold quantile of 0.999 was determined to be an appropriate compromise in terms of
 226 removing obviously outlier points, yet retaining physically plausible results.

227
 228 A scatter plot of SWE vs. h for the uncleaned SNOTEL dataset from CONUS and AK reveals many non-physical
 229 points, mostly when a very large h is reported for a very low SWE (Figure 4a). Approximately 0.7% of the original
 230 data points were removed in the cleaning process described above, creating a more physically plausible scatter plot
 231 (Figure 4b). Note that the outlier detection process was applied to each station individually. The same procedure was
 232 applied to the BC and northeast USA data sets as well (not shown). Table 1 summarizes useful information about
 233 the numerous data sets described above and indicates the final number of data points retained for each.

234

235 Table 1: Summary of information about the datasets used in this study. The numbers of stations and data points
 236 reflect the post-processed data.

Dataset Name	Dataset Type	Number of retained stations	Number of retained data points	Precision (h / SWE)
NRCS SNOTEL	Snow pillow (SWE),	791	1,900,000	(0.5 in / 0.1 in)
NRCS SCAN	ultrasonic (h)	5	7094	(0.5 in / 0.1 in)
British Columbia Snow Survey	Snow pillow (SWE), ultrasonic (h)	31	61,000	(1 cm / 1 mm)
Maine Geological Survey	Adirondack or Federal sampler (SWE and h)	431	28,000	(0.5 in / 0.5 in)
Hubbard Brook (Station 2), NH	Mount Rose sampler (SWE and h)	1	704	(0.1 in / 0.1 in)
Thompson Farm, NH	Snow core (SWE and h)	2	988	0.5 in / 0.5 in
Sleepers River, VT	Adirondack sampler	14	7214	(0.5 in / 0.5 in)
New York Snow Survey	Adirondack or Federal sampler (SWE and h)	523	44,614	(0.5 in / 0.5 in)
Chugach Mountains, AK	Federal sampler (SWE and h) and avalanche probe (h)	71	71	(0.5 in / 0.5 in) for sampler; 1 cm for probe

237

238 2.1.2 Climatological Variables

239 30-year climate normals at 800 m (nominal) resolution for CONUS and for the period 1981-2010 were obtained
 240 from the PRISM website (Daly et al., 1994). PRISM normals for British Columbia (BC), Canada, were obtained
 241 from the ClimateBC project (Wang et al., 2012), also for the 1981-2010 period. Finally, PRISM normals for Alaska
 242 (AK) were obtained from the Integrated Resource Management Applications (IRMA) Portal run by the National



243 Park Service. The AK normals are for the 1971-2000 period and have a slightly coarser resolution (approximately
244 1.5 km). Figure 5 shows gridded maps of mean annual precipitation (*MAP*) and mean February Temperature (\bar{T}_F)
245 for these three climate products, plotted together. Other temperature products (max and min temperatures; other
246 months) were obtained as well, but are not shown.

247

248 **2.2 Regression Model**

249 In order to demonstrate the varying degrees of influence of explanatory variables, several regression models were
250 constructed. In each case, the model was built by randomly selecting 50% of the paired SWE-*h* measurements from
251 the aggregated CONUS, AK, and BC snow pillow datasets. The model was then validated by applying it to the
252 remaining 50% of the dataset and comparing the modeled SWE to the observed SWE for those points. Additional
253 validation was done with the northeast USA datasets which were completely left out of the model building process.

254

255 **2.2.1 One-Equation Model**

256 The simplest equation, and one that is supported by the strong correlation seen in Figure 3, is one that expresses
257 SWE as a function of *h*. A linear model is attractive in terms of simplicity, but this limits the snowpack to a constant
258 density. An alternative is to express SWE as a power law, i.e.,

259

$$260 \quad (1) \quad SWE = Ah^{a_1}.$$

261

262 This equation can be log-transformed into

263

$$264 \quad (2) \quad \log_{10}(SWE) = \log_{10}(A) + a_1 \log_{10}(h)$$

265

266 which immediately allows for simple linear regression methods to be applied. With both *h* and SWE expressed in
267 units of mm, the obtained coefficients are $(A, a_1) = (0.146, 1.102)$. Information on the performance of the model
268 will be deferred until the results section.

269

270 **2.2.2 Two-Equation Model**

271 Recall from Figures 1 and 4 that there is a hysteresis loop in the SWE-*h* relationship. During the accumulation
272 phase, snow densities are relatively low. During the ablation phase, the densities are relatively high. So, the same
273 snowpack depth is associated with two different SWEs, depending upon the time of year. The regression equation
274 given above does not resolve this difference. This can be addressed by developing two separate regression
275 equations, one for the accumulation (*acc*) and one for the ablation (*abl*) phase. This approach takes the form

276

$$277 \quad (3) \quad SWE_{acc} = Ah^{a_1}; \quad DOY < DOY^*$$

278

$$279 \quad (4) \quad SWE_{abl} = Bh^{b_1}; \quad DOY \geq DOY^*$$



280
 281 where DOY is the number of days from the start of the water-year (October 1 is the origin), and DOY^* is the critical
 282 or dividing day-of-water-year separating the two phases. Put another way, DOY^* is the day of peak SWE.
 283 Interannual variability results in a range of DOY^* for a given site. Additionally, some sites, particularly the SCAN
 284 sites in the northeast USA, demonstrate multi-peak SWE profiles in some years. To reduce model complexity,
 285 however, we investigated the use of a simple climatological (long term average) value of DOY^* . For each snow
 286 pillow station, the average DOY^* was computed over the period of record of that station. Analysis of all of the
 287 stations revealed that this average DOY^* was relatively well correlated with the climatological mean April maximum
 288 temperature (the average of the daily maximums recorded in April; $R^2 = 0.7$). However, subsequent regression
 289 analysis demonstrated that the SWE estimates were relatively insensitive to DOY^* and the best results were actually
 290 obtained when DOY^* was uniformly set to 180 for all stations. Again, with both SWE and h in units of mm, the
 291 regression coefficients turn out to be $(A, a_1) = (0.150, 1.082)$ and $(B, b_1) = (0.239, 1.069)$.

292
 293 As these two equations are discontinuous at DOY^* , they are blended smoothly together to produce the final two-
 294 equation model

295
 296 (5)
$$SWE = SWE_{acc} \frac{1}{2} (1 - \tanh[0.01\{DOY - DOY^*\}]) +$$

 297
$$SWE_{abl} \frac{1}{2} (1 + \tanh[0.01\{DOY - DOY^*\}])$$

298
 299 The coefficient 0.01 in the tanh function controls the width of the blending window and was selected to minimize
 300 the root mean square error of the model estimates.

301
 302 **2.2.3 Two-Equation Model with Climate Parameters**

303 A final model was constructed by incorporating climatological variables. Again, the emphasis is this study is on
 304 methods that can be implemented at locations lacking the time series of weather variables that might be available at
 305 a weather or SNOTEL station. Climatological normals are unable to account for interannual variability, but they do
 306 preserve the high spatial gradients in climate that can lead to spatial gradients in snowpack characteristics. Stepwise
 307 linear regression was used to determine which variables to include in the regression. The initial list of potential
 308 variables included was

309
 310 (6)
$$SWE = f(h, z, MAP, \bar{T}_{J_{min}}, \bar{T}_{J_{mean}}, \bar{T}_{J_{max}}, \bar{T}_{F_{min}}, \bar{T}_{F_{mean}}, \bar{T}_{F_{max}}, \bar{T}_{M_{min}}, \bar{T}_{M_{mean}}, \bar{T}_{M_{max}}, \bar{T}_{A_{min}}, \bar{T}_{A_{mean}}, \bar{T}_{A_{max}})$$

311
 312 where z is the elevation (m), MAP is the mean annual precipitation (mm) and the temperatures ($^{\circ}C$) represent the
 313 mean of minimum, mean, and maximum daily values for the months January through April (J, F, M, A). For
 314 example, $\bar{T}_{J_{min}}$ is the climatological normal of the average of the daily minimum temperatures observed in January.



315 In the stepwise regression, explanatory variables were accepted if they improved the adjusted R^2 value by 0.001.

316 The result of the regression yielded

317

318 (7) $SWE_{acc} = Ah^{a_1}MAP^{a_2}(\bar{T}_{F_{mean}} + 30)^{a_3}; \quad DOY < DOY^*$

319

320 (8) $SWE_{abl} = Bh^{b_1}MAP^{b_2}(\bar{T}_{F_{mean}} + 30)^{b_3}; \quad DOY \geq DOY^*$

321

322 or, in log-transformed format,

323

324 (9) $\log_{10}(SWE_{acc}) = \log_{10}(A) + a_1 \log_{10}(h) +$
325 $a_2 \log_{10}(MAP) + a_3 \log_{10}(\bar{T}_{F_{mean}} + 30); \quad DOY < DOY^*$

326

327 (10) $\log_{10}(SWE_{abl}) = \log_{10}(B) + b_1 \log_{10}(h) +$
328 $b_2 \log_{10}(MAP) + b_3 \log_{10}(\bar{T}_{F_{mean}} + 30); \quad DOY \geq DOY^*$

329

330 indicating that only snow depth, mean annual precipitation and mean February temperature were relevant. Manual
331 tests of model construction with other variables included confirmed that Eqns. (7-8) yielded the best results. In the
332 above equations, note that an offset is added to the temperature in order to avoid taking the log of a negative
333 number. These two SWE estimates for the individual (*acc* and *abl*) phases of the snowpack are then blended with
334 Eqn. (5) to produce a single equation for SWE spanning the entire water year. The obtained regression coefficients
335 were $(A, a_1, a_2, a_3) = (0.0128, 1.070, 0.132, 0.506)$ and $(B, b_1, b_2, b_3) = (0.0271, 1.038, 0.201, 0.310)$. The
336 physical interpretation of these coefficients is straightforward. The fact that the coefficients on depth are greater than
337 unity indicates that the density (SWE/h) increases as the snowpack depth increases. The positive coefficients
338 associated with *MAP* and $\bar{T}_{F_{mean}}$ indicate that snow densities should be higher in warmer, wetter locations than in
339 colder, drier locations.

340 3 Results

341 A comparison of the three regression models (one-equation model, Eq. (2); two-equation model, Eqs. (3-5); multi-
342 variable two-equation model, Eqs. (5, 7-8)) is provided in Figure 6. The left column shows scatter plots of modeled
343 SWE to observed SWE for the validation data set with the 1:1 line shown in black. The right column shows
344 histograms of the model residuals. The vertical lines in the right column show the mean error, or model bias.
345 Visually, it is clear that the one-equation model performs relatively poorly with a large negative bias. This is easily
346 explained. The SNOTEL measurements are uniformly spaced in time (daily). Given that the accumulation season is
347 much longer than the ablation season (Figure 1), there are many more data points that are representative of the
348 accumulation season. The model fit is weighted towards these points, which leads to large negative residuals in the
349 ablation season. This large negative bias is partially overcome by the two-equation model (middle row, Figure 6).
350 The cloud of points is closer to the 1:1 line and the vertical black line indicating the mean error is closer to zero. In



351 the final row of Figure 6, we see that the multi-variable two-equation model yields the best result by far. The
 352 residuals are now evenly distributed with a negligible bias. Several metrics of performance for the three models,
 353 including R^2 (Pearson coefficient), bias, and root-mean-square-error (RMSE), are provided in Table 2.

354

355 Table 2: Summary of performance metrics for the three regression models presented in Section 2.2.

Model	R^2	Bias (mm)	RMSE (mm)
One-equation	0.946	-19.5	102
Two-equation	0.962	-5.1	81
Multi-variable two-equation	0.972	-0.5	67

356

357 Model errors will have varying impact on the local snow regime depending on the total precipitation in a specific
 358 region. Therefore, an RMSE was computed at each station location and normalized by the PRISM estimate of MAP
 359 at that location. Figure 7 shows the probability density function of these normalized errors. The average RMSE is
 360 approximately 5% of MAP , with most falling into the range of 2-8%. The spatial distribution of these normalized
 361 errors is shown in Figure 8. For the SNOTEL stations, there are no clear regional patterns governing the normalized
 362 errors, with the possible exception of the Sierra Nevada, where the errors are consistently higher than elsewhere.
 363 The British Columbia stations also show higher overall errors.

364

365 3.1 Results for Snow Classes

366 A key objective of this study is to regress climatological information in a continuous rather than a discrete way. The
 367 work by Sturm et al. (2010) therefore provides a valuable point of comparison. In that study, the authors developed
 368 the following equation for density ρ_b

369

$$370 \quad (11) \quad \rho_b = (\rho_{max} - \rho_0) [1 - e^{(-k_1 h - k_2 DOY)}] + \rho_0$$

371

372 where ρ_0 is the initial density, ρ_{max} is the maximum or ‘final’ density (end of water year), k_1 and k_2 are coefficients,
 373 and DOY in this case begins on January 1. This means that their DOY for October 1 is -92. The coefficients vary
 374 with snow class and the values determined by Sturm et al. (2010) are shown in Table 3.

375

376 Table 3: Model parameters by snow class for Sturm et al. (2010).

Snow Class	ρ_{max}	ρ_0	k_1	k_2
Alpine	0.5975	0.2237	0.0012	0.0038
Maritime	0.5979	0.2578	0.0010	0.0038
Prairie	0.5941	0.2332	0.0016	0.0031
Tundra	0.3630	0.2425	0.0029	0.0049
Taiga	0.2170	0.2170	0.0000	0.0000

377



378 To make a comparison, the snow class for each SNOTEL (including CONUS, AK, and BC) site was determined
 379 using a 1-km snow class grid (Sturm et al., 2010) and Equation (11) was used to estimate snow density (and then
 380 SWE) for every point in the validation dataset described in Section 2.2. Figure 9 compares the SWE estimates from
 381 the Sturm model and from the present multi-variable, two-equation model (Equations 5, 7-8). The upper left panel of
 382 Figure 9 shows all of the data, and the remaining panels show the results for each snow class. In all cases, the
 383 current model provides better estimates. Plots of the residuals by snow class are provided in Figure 10, giving an
 384 indication of the bias of each model for each snow class. Summaries of the model performance, broken out by snow
 385 class, are given in Table 4.

386

387 Table 4: Comparison of model performance by Sturm et al. (2010) and the present study.

Model Snow Class	Sturm et al. (2010)			Multi-variable two-equation model		
	R ²	Bias (mm)	RMSE (mm)	R ²	Bias (mm)	RMSE (mm)
All Data	0.928	-29.2	111	0.972	-0.5	67
Alpine	0.973	10.1	55	0.971	-0.3	55
Maritime	0.968	-16.8	109	0.970	-4.5	105
Prairie	0.967	18.7	56	0.965	-0.2	51
Tundra	0.956	-10.5	82	0.969	-6.1	67
Taiga	0.943	-80.0	151	0.971	2.4	62

388

389 3.2 Results for Northeast USA

390 The regression equations in this study were developed using a large collection of SNOTEL sites in CONUS, AK,
 391 and BC. The snow pillow sites are limited to locations west of approximately W 105° (Figure 2a). By design, the
 392 data sets from the northeastern USA (Section 2.1.1.3) were left as an entirely independent validation set. These
 393 northeastern sites are geographically distant from the training data sets, are subject to a very different climate, and
 394 are generally at much lower elevations than the western sites, providing an interesting opportunity to test how robust
 395 the present model is.

396

397 Figure 11 graphically summarizes the datasets and the performance of the multi-variable two-equation model of the
 398 current study. The RMSE values are comparable to those found for the western stations, but, given the
 399 comparatively thinner snowpacks in the northeast, represent a larger relative error (Table 5). The bias of the model
 400 is consistently positive, in contrast to the western stations where the bias was negligible.

401

402 Table 5: Performance metrics for the multi-variable two-equation model applied to various northeastern USA
 403 datasets.

Dataset Name	R ²	Bias (mm)	RMSE (mm)
Maine Geological Survey, ME	0.91	8.9	33.3
Hubbard Brook (Station 2), NH	0.63	18.9	64.2
Thompson Farm, NH	0.85	7.1	21.6
NRCS SCAN	0.87	-1.8	38.7
Sleepers River, VT	0.93	14.0	29.7
New York Snow Survey	0.93	13.8	31.2



404

405 **3.3 Results for Chugach Mountains**

406 The results for the Federal sampler core measurements in the Chugach Mountains are shown in Figure 12, using a
407 format consistent with Figure 11. The three different measurement campaigns (March, April, and May) can be seen
408 by the different symbol colors in the left panel. One notable difference between Figures 11 and 12 is that the
409 Chugach dataset only spans spring months and not the full water year. So, the cluster of data points does not start at
410 the origin. The R2, bias (mm) and RMSE (mm) are 0.89, -50.0 and 118.0, respectively.

411 **4 Discussion**

412 The results presented in this study show that the regression equation described by equations (5, 7-8) is an
413 improvement (lower bias and RMSE) over other widely used bulk density equations. The key advantage is that the
414 present method regresses in relevant physical parameters directly, rather than using discrete bins (for snow class,
415 elevation, month of year, etc.), each with its own set of model coefficients. The comparison (Figs. 9-10; Table 4) to
416 the model of Sturm et al. (2010) reveals a peculiar behavior of that model for the Taiga snow class, with a large
417 negative bias in the Sturm estimates. Inspection of the coefficients provided for that class (Table 3) shows that the
418 model simply predicts that $\rho_b = \rho_{max} = 0.217$ for all conditions.

419

420 When our multi-variable two-equation model, developed solely from western North American data, is applied to
421 northeast USA locations, it produces SWE estimates with smaller RSME values and larger biases than the western
422 stations. When comparing the SWE- h curves of the SNOTEL data (Figure 4b) to those of the east coast data sets
423 (left column; Figure 11), it is clear that the northeast data generally have more scatter. This is confirmed by
424 computing the correlation coefficients between SWE and h for each dataset. It is unclear if this disparity in
425 correlation is related to measurement methodology or is instead a ‘signal to noise’ issue. Comparing Figures 4 and
426 11 shows the considerable difference in snowpack depth between the western and northeastern data sets. When the
427 western dataset is filtered to include only measurement pairs where $h < 1.5$ m, the correlation coefficient is reduced
428 to a value consistent with the northeast datasets. This suggests that the performance of the current (or other)
429 regression model is not as good at shallow snowpack depths. This is also suggested upon examination of the time
430 series of observed $\rho_b = SWE/h$ for a given season at a snow pillow site. Very early in the season, when the depths
431 are small, the density curve is very noisy. Later in the season, when depths are greater, the density curve becomes
432 much smoother.

433

434 When applied to the Chugach coring measurements, the model appears to perform well. The higher values of bias
435 and RMSE (when compared to Tables 4 and 5) are higher in part since the measurements (and model estimates) of
436 SWE are only at times of larger snow depth. The variability of the Chugach avalanche probe measurements was
437 assessed by taking the standard deviation of 8 h measurements per site. The average of this standard deviation over
438 the sites was 22 cm and the average coefficient of variation (standard deviation normalized by the mean) over the
439 sites was 15%. Propagating this uncertainty through the regression equations yields a slightly higher (16%)
440 uncertainty in the SWE estimates. Clearly, this is a function of surface roughness of the underlying terrain.



441 Backcountry areas characterized by fields and meadows are likely to have smaller coefficients of variation for
442 ensembles of depth measurements over a small radius. As a result, SWE estimated from a single depth measurement
443 should be comparatively accurate. Areas of high surface roughness, characterized by crags, rocks and fallen logs
444 will have large coefficients of variation and larger numbers of depth measurements should be collected and averaged
445 to provide the best possible SWE estimate.

446
447 Measurement precision also affects the construction of a regression model. Upon inspection of the data, it was
448 observed that the precision of the depth measurements was approximately 25 mm and that of the SWE
449 measurements was approximately 2.5 mm. To test the sensitivity of the model coefficients to the measurement
450 precision, the depth values in the training dataset were randomly perturbed by +/- 25 mm and the SWE values were
451 randomly perturbed by +/- 2.5 mm and the regression coefficients were recomputed. This process was repeated
452 numerous times and the mean values of the perturbed coefficients were found to be $(A, a_1, a_2, a_3) =$
453 $(0.0188, 0.9737, 0.2034, 0.4301)$ and $(B, b_1, b_2, b_3) = (0.0386, 0.9535, 0.2745, 0.2184)$. These adjusted
454 coefficients were then used to recompute the SWE values for the validation data set and the bias and RMSE were
455 found to be -10.5 mm and 72.7 mm. This represents a roughly 10% increase in RMSE, but a considerable increase in
456 bias magnitude (see Table 4 for the original values). This sensitivity of the regression analysis to measurement
457 precision underscores the need to have high-precision measurements for the training data set. It also raises the
458 interesting question of whether or not future resources should be directed towards expanding networks (greater
459 spatial coverage) of current technologies or towards refining instrumentation (better accuracy) at currently
460 instrumented stations.

461
462 Another important consideration has to do with the uncertainty of depth measurements that the model is applied to.
463 For context, one application of this study is to crowd-sourced, opportunistic snow depth measurements from
464 programs like the Community Snow Observations (CSO; Hill et al., 2018) project. In the CSO program,
465 backcountry recreational users submit depth measurements, typically taken with an avalanche probe, using a
466 smartphone in the field. The measurements are then converted to SWE estimates which are assimilated into
467 snowpack models. These depth measurements are ‘any time, any place’ in contrast to repeated measurements from
468 the same location, like snow pillows or snow courses. Most avalanche probes have cm-scale graduated markings, so
469 measurement precision is not a major issue. A larger problem is the considerable variability in snowpack depth that
470 can exist over short (meter scale) distances. Recalling the Chugach discussion above, even in flat areas, with a
471 smooth snow surface (away from major drifting or wind scour), terrain features such as rocks, logs, and vegetation
472 can produce large variations in probe measurements.

473
474 Expansion of CSO measurements in areas lacking SWE measurements can increase our understanding of the
475 extreme spatial variability in snow distribution and the inherent uncertainties associated with modeling SWE in
476 these regions. It could also prove useful for estimating watershed-scale SWE in regions like the northeastern USA,
477 which is currently limited to five automated SCAN sites with historical SWE measurements for only the past two



478 decades. Additionally, historical snow depth measurements are more widely available in the Global Historical
479 Climatology Network (GHCN-Daily; Menne et al. 2012), with several records extending back to the late 1800s.
480 While many of the GHCN stations are confined to lower elevations with shallower snow depths, the broader
481 network of quality-controlled snow depth data paired with daily GHCN temperature and precipitation measurements
482 could potentially be used to reconstruct SWE in the eastern US given additional model development and refinement.

483 **5 Conclusions**

484 We have developed a new, easy to use method for converting snow depth measurements to snow water equivalent
485 estimates. The key difference between our approach and previous approaches is that we directly regress in
486 climatological variables in a continuous fashion, rather than a discrete one. Given the abundance of freely available
487 climatological norms, a depth measurement tagged with coordinates (latitude and longitude) and a time stamp is
488 easily and immediately converted into SWE.

489
490 We developed this model with data from paired SWE-*h* measurements from the western United States and British
491 Columbia. The model was tested against entirely independent data (primarily snow course; some snow pillow) from
492 the northeastern United States and was found to perform well, albeit with larger biases and root-mean-squared-
493 errors. The model was tested against other well-known regression equations and was found to perform better.

494
495 This model is not a replacement for more sophisticated snow models that evolve the snowpack based on high
496 frequency (e.g., daily or sub-daily) weather data inputs. The intended purpose of this model is to constrain SWE
497 estimates in circumstances where snow depth is known, but weather variables are not, a common issue in sparsely
498 instrumented areas in North America.

499 **6 Acknowledgements**

500 Support for this project was provided by NASA (NNX17AG67A). R. Crumley acknowledges support from the
501 CUAHSI Pathfinder Fellowship. E. Burakowski acknowledges support from NSF (MSB-ECA #1802726).

502 **7 Data Access**

503 Numerous online datasets were used for this project and were obtained from the following locations:

- 504 1. NRCS Snow Telemetry: <https://www.wcc.nrcs.usda.gov/snow/SNOTEL-wedata.html>
- 505 2. NRCS Soil Climate Analysis Network: <https://www.wcc.nrcs.usda.gov/scan/>
- 506 3. British Columbia Automated Snow Weather Stations:
507 [https://www2.gov.bc.ca/gov/content/environment/air-land-water/water/water-science-data/water-data-](https://www2.gov.bc.ca/gov/content/environment/air-land-water/water/water-science-data/water-data-tools/snow-survey-data/automated-snow-weather-station-data)
508 [tools/snow-survey-data/automated-snow-weather-station-data](https://www2.gov.bc.ca/gov/content/environment/air-land-water/water/water-science-data/water-data-tools/snow-survey-data/automated-snow-weather-station-data)
- 509 4. Maine Cooperative Snow Survey: <https://mgs-maine.opendata.arcgis.com/datasets/maine-snow-survey-data>
- 510 5. New York Snow Survey: <http://www.nrcc.cornell.edu/regional/snowsury/snowsury.html>
- 511 6. Sleepers River Research Watershed. Snow data not available online; request data from contact at:
512 <https://nh.water.usgs.gov/project/sleepers/index.htm>



- 513 7. Hubbard Brook Experimental Forest: <https://hubbardbrook.org/d/hubbard-brook-data-catalog>
514 8. CONUS PRISM Data: <http://www.prism.oregonstate.edu/>
515 9. British Columbia PRISM Data: <http://climatebcdata.climatewna.com/>
516 10. Alaska PRISM Data: <https://irma.nps.gov/Portal/>
517
518 A Matlab function for calculating SWE based on the results is this paper has been made publicly available at Github
519 (URL provided upon paper acceptance).



520 **References**

521

522 Alford, D.: Density variations in alpine snow, *J. Glaciol.*, 6(46), 495-503,

523 <https://doi.org/10.3189/S0022143000019717>, 1967.

524

525 Avanzi, F., De Michele, C., and Ghezzi, A.: On the performances of empirical regressions for the estimation of bulk
526 snow density, *Geogr. Fis. Dinam. Quat.*, 38, 105-112, doi:10.4461/GFDQ.2015.38.10, 2015.

527

528 Beaumont, R.: Mt. Hood pressure pillow snow gage, *J. Appl. Meteorol.*, 4, 626-631, [https://doi.org/10.1175/1520-0450\(1965\)004<0626:MHPPSG>2.0.CO;2](https://doi.org/10.1175/1520-0450(1965)004<0626:MHPPSG>2.0.CO;2) 1965.

529

531 Beaumont, R., and Work, R.: Snow sampling results from three samplers, *Hydrol. Sci. J.*, 8(4), 74-78,

532 <https://doi.org/10.1080/02626666309493359>, 1963.

533

534 Burakowski, E.A., Ollinger, S., Lepine, L., Schaaf, C.B., Wang, Z., Dobb, J.E., Hollinger, D.Y., Kim, J.-H., Erb, A.,
535 and Martin, M.E.: Spatial scaling of reflectance and surface albedo over a mixed-use, temperate forest landscape
536 during snow-covered periods, *Remote Sens. Environ.*, 158, 465-477, <https://doi.org/10.1016/j.rse.2014.11.023>,
537 2015.

538

539 Burakowski, E.A., Wake, C.P., Stampone, M., and Dobb, J.: Putting the Capital 'A' in CoCoRAHS: An
540 Experimental Program to Measure Albedo using the Community Collaborative Rain Hail and Snow (CoCoRaHS)
541 Network, *Hydrol. Process.*, 27(21), 3024-3034, <https://doi.org/10.1002/hyp.9825>, 2013.

542

543 Campbell, J., Ollinger, S., Flerchinger, G., Wicklein, H., Hayhoe, K., and Bailey, A.: Past and projected future
544 changes in snowpack and soil frost at the Hubbard Brook Experimental Forest, New Hampshire, USA, *Hydrol.*
545 *Process.*, 24, 2465-2480, <https://doi.org/10.1002/hyp.7666>, 2010.

546

547 Church, J.E.: Snow surveying: its principles and possibilities, *Geogr. Rev.*, 23(4), 529-563, DOI: 10.2307/209242,
548 1933.

549

550 Daly, C., Neilson, R., and Phillips, D.: A statistical-topographic model for mapping climatological precipitation over
551 mountainous terrain, *J. Appl. Meteorol.*, 33, 140-158, [https://doi.org/10.1175/1520-0450\(1994\)033<0140:ASTMFM>2.0.CO;2](https://doi.org/10.1175/1520-0450(1994)033<0140:ASTMFM>2.0.CO;2), 1994.

552

554 Deeb, E., Marshall, H.-P., Forster, R., Jones, C., Hiemstra, C., and Siqueira, P.: Supporting NASA SnowEx remote
555 sensing strategies and requirements for L-band interferometric snow depth and snow water equivalent estimation,



- 556 Proceedings of the 2017 IEEE International Geoscience and Remote Sensing Symposium, Fort Worth, TX, 1395-
557 1396, DOI: 10.1109/IGARSS.2017.8127224, 2017.
- 558
- 559 Dixon, D., and Boon, S.: Comparison of the SnowHydro sampler with existing snow tube designs, *Hydrol. Process.*,
560 26(17), 2555-2562, <https://doi.org/10.1002/hyp.9317>, 2012.
- 561
- 562 Dressler, K., Fassnacht, S., and Bales, R.: A comparison of snow telemetry and snow course measurements in the
563 Colorado River basin, *J. Hydrometeorol.*, 7, 705-712, <https://doi.org/10.1175/JHM506.1>, 2006.
- 564
- 565 Fick, S., and Hijmans, R.: WorldClim2: new 1-km spatial resolution climate surfaces for global land areas,” *Int. J.*
566 *Climatol.*, 37, 4302-4315, <https://doi.org/10.1002/joc.5086>, 2017
- 567
- 568 Goodison, B., Glynn, J., Harvey, K., and Slater, J.: Snow Surveying in Canada: A Perspective, *Can. Water Resour.*
569 *J.*, 12(2), 27-42, <https://doi.org/10.4296/cwrj1202027>, 1987.
- 570
- 571 Gnanadesikan, R., and Kettenring, J.: Robust estimates, residuals, and outlier detection with multiresponse data,
572 *Biometrics*, 28, 81-124, DOI: 10.2307/2528963, 1972.
- 573
- 574 Hill, D.F., Wolken, G. J., Wikstrom Jones, K., Crumley, R., and Arendt, A.: Crowdsourcing snow depth data with
575 citizen scientists, *Eos*, 99, <https://doi.org/10.1029/2018EO108991>, 2018.
- 576
- 577 Jonas, T., and Magnusson, M.: Estimating the snow water equivalent from snow depth measurements, *J. Hydrol.*,
578 378, 161-167, <https://doi.org/10.1016/j.jhydrol.2009.09.021>, 2009.
- 579
- 580 Kang, D.H., and Barros, A.P.: Full-system testing in laboratory conditions of an L-band snow sensor system for in
581 situ monitoring of snow-water content, *IEEE Trans. Geosci. Remote Sens.*, 49(3), 908-919,
582 10.1109/TGRS.2010.2072786, 2011.
- 583
- 584 Leinss, S., Wiesmann, A., Lemmetyinen, J., and Hajnsek, I.: Snow water equivalent measured by differential
585 interferometry, *IEEE J. Sel. Top. Appl. Earth Obs. Remote Sens.*, 8(8), 3773-3790, 10.1109/JSTARS.2015.2432031,
586 2015.
- 587
- 588 Leys, C., Klein, O., Dominicy, Y., and Ley, C.: Detecting multivariate outliers: use a robust variant of the
589 Mahalanobis distance, *J. Exp. Soc. Psychol.*, 74, 150-156, <https://doi.org/10.1016/j.jesp.2017.09.011>, 2018.
- 590



- 591 Liang, X., Lettermaier, D., Wood, E., and Burges, S.: A simple hydrologically based model of land surface water
592 and energy fluxes for general circulation models, *J. Geophys. Res. Atmos.*, 99(D7), 14,415-14,428,
593 <https://doi.org/10.1029/94JD00483>, 1994.
594
- 595 Liston, G., and Elder, K.: A distributed snow evolution modeling system (SnowModel), *J. Hydrometeorol.*, 7, 1259-
596 1276, <https://doi.org/10.1175/JHM548.1>, 2006.
597
- 598 Lundberg, A., Richardson-Naslund, C., and Andersson, C.: Snow density variations: consequences for ground
599 penetrating radar, *Hydrol. Process.*, 20, 1483-1495, <https://doi.org/10.1002/hyp.5944>, 2006.
600
- 601 Maine Geological Survey: Maine Cooperative Snow Survey Dataset,
602 https://www.maine.gov/dacf/mgs/hazards/snow_survey/, 2018.
603
- 604 De Maesschalck, R., Jouan-Rimbaud, D., and Massart, D.: The Mahalanobis distance, *Chemometr. Intell. Lab. Syst.*,
605 50(1), 1-18, [https://doi.org/10.1016/S0169-7439\(99\)00047-7](https://doi.org/10.1016/S0169-7439(99)00047-7), 2000.
606
- 607 McCreight, J., and Small, E.: Modeling bulk density and snow water equivalent using daily snow depth
608 observations, *The Cryosphere*, 8, 521-536, <https://doi.org/10.5194/tc-8-521-2014>, 2014.
609
- 610 Meloyund, V., Leira, B., Hoiseth, K., and Liso, K.: Predicting snow density using meteorological data, *Meteorol.*
611 *Appl.*, 14, 413-423, <https://doi.org/10.1002/met.40>, 2007.
612
- 613 Menne, M.J., I. Durre, R.S. Vose, B.E. Gleason, and Houston, T.G.: An overview
614 of the Global Historical Climatology Network-Daily Database, *J. Atmos. Ocean. Technol.*, 29, 97-910,
615 doi:10.1175/JTECH-D-11-00103.1, 2012.
616
- 617 Molotch, N.P., and Bales, R.C.: SNOTEL representativeness in the Rio Grande headwaters on the basis of
618 physiographics and remotely sensed snow cover persistence, *Hydrol. Process.*, 20(4), 723-739,
619 <https://doi.org/10.1002/hyp.6128>, 2006.
620
- 621 Mote, P., Li, S., Lettermaier, D., Xiao, M., and Engel, R.: Dramatic declines in snowpack in the western US,” *npj*
622 *Clim. Atmos. Sci.*, 1(2), 1-6, doi:10.1038/s41612-018-0012-1, 2018.
623
- 624 Mizukami, N., and Perica, S.: Spatiotemporal characteristics of snowpack density in the mountainous regions of the
625 western United States, *J. Hydrometeorol.*, 9, 1416-1426, <https://doi.org/10.1175/2008JHM981.1>, 2008.
626
- 627 New York Snow Survey, NOAA, Northeast Regional Climate Center at Cornell University, 2018.



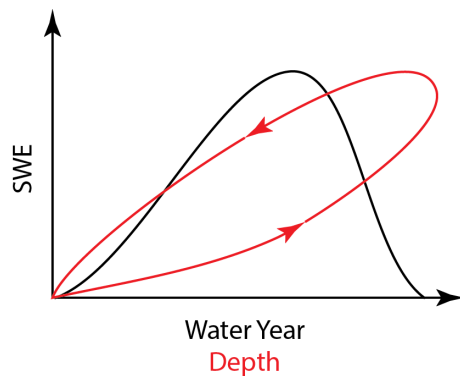
- 628
629 Pagano, T., Garen, D., Perkins, T., and Pasteris, P.: Daily updating of operational statistical seasonal water supply
630 forecasts for the western U.S., *J. Am. Water Resour. Assoc.*, 45(3), 767-778, <https://doi.org/10.1111/j.1752->
631 1688.2009.00321.x, 2009.
632
633 Painter, T., Berisford, D., Boardman, J., Bormann, K., Deems, J., Gehrke, F., Hedrick, A., Joyce, M., Laidlaw, R.,
634 Marks, D., Mattmann, C., McGurk, B., Ramirez, P., Richardson, M., Skiles, S., Seidel, F., and Winstral, A.: The
635 Airborne Snow Observatory: fusion of scanning lidar, imaging spectrometer, and physically-based modeling for
636 mapping snow water equivalent and snow albedo, *Remote Sens. Environ.*, 184, 139-152,
637 doi:10.1016/j.rse.2016.06.018, 2016.
638
639 Pistocchi, A.: Simple estimation of snow density in an Alpine region, *J. Hydrol. Reg. Stud.*, 6, 82-89,
640 <http://dx.doi.org/10.1016/j.ejrh.2016.03.004>, 2016.
641
642 Rousseeuw, P.: Least Median of Squares Regression, *J. Am. Stat. Assoc.*, 79, 871-880, DOI:
643 10.1080/01621459.1984.10477105, 1984.
644
645 Ryan, W., Doesken, N., and Fassnacht, S.: Evaluation of Ultrasonic Snow Depth Sensors for U.S. Snow
646 Measurements, *J. Atmos. Ocean. Technol.*, 25, 667-684, <https://doi.org/10.1175/2007JTECHA947.1>, 2008.
647
648 Schaefer, G., Cosh, M., and Jackson, T.: The USDA Natural Resources Conservation Service Soil Climate Analysis
649 Network (SCAN), *J. Atmos. Ocean. Technol.*, 24, 2073-2077, <https://doi.org/10.1175/2007JTECHA930.1>, 2007.
650
651 Serreze, M., Clark, M., Armstrong, R., McGinnis, D., and Pulwarty, R.: Characteristics of the western United States
652 snowpack from snowpack telemetry (SNOTEL) data, *Water Resour. Res.*, 35(7), 2145-2160,
653 <https://doi.org/10.1029/1999WR900090>, 1999.
654
655 Shanley, J., and Chalmers, A.: The effect of frozen soil on snowmelt runoff at Sleepers River, Vermont, *Hydrol.*
656 *Process.*, 13(12-13), 1843-1857, [https://doi.org/10.1002/\(SICI\)1099-1085\(199909\)13:12<1843::AID-](https://doi.org/10.1002/(SICI)1099-1085(199909)13:12<1843::AID-)
657 [HYP879>3.0.CO;2-G](https://doi.org/10.1002/(SICI)1099-1085(199909)13:12<1843::AID-HYP879>3.0.CO;2-G), 1999.
658
659 Sokol, J., Pultz, T., and Walker, A.: Passive and active airborne microwave remote sensing of snow cover,” *Int.*
660 *J. Remote. Sens.*, 24, 5327-5344, <https://doi.org/10.1080/0143116031000115076>, 2003.
661
662 Sturm, M., Holmgren, J., and Liston, G.: A seasonal snow cover classification system for local to global
663 applications, *J. Clim.*, 8, 1261-1283, [https://doi.org/10.1175/1520-0442\(1995\)008<1261:ASSCCS>2.0.CO;2](https://doi.org/10.1175/1520-0442(1995)008<1261:ASSCCS>2.0.CO;2), 1995.
664



- 665 Sturm, M., Taras, B., Liston, G.E., Derksen, C., Jonas, T., and Lea, J.: Estimating snow water equivalent using snow
666 depth data and climate classes, *J. Hydrometeorol.*, 11, 1380-1394, <https://doi.org/10.1175/2010JHM1202.1>, 2010.
667
- 668 Vuyovich, C., Jacobs, J., and Daly, S.: Comparison of passive microwave and modeled estimates of total watershed
669 SWE in the continental United States, *Water Resour. Res.*, 50(11), 9088-9012,
670 <https://doi.org/10.1002/2013WR014734>, 2014.
671
- 672 Wang, T., Hamann, A., Spittlehouse, D.L., and Murdock, T.: ClimateWNA - High-Resolution Spatial Climate Data
673 for Western North America, *J. Appl. Meteorol. Climatol.*, 51, 16-29, <https://doi.org/10.1175/JAMC-D-11-043.1>,
674 2012.
675
- 676 Wigmosta, M.S., Vail, L., and Lettenmaier, D.: A distributed hydrology-vegetation model for complex
677 terrain, *Water Resour. Res.*, 30, 1665-1679, <https://doi.org/10.1029/94WR00436>, 1994



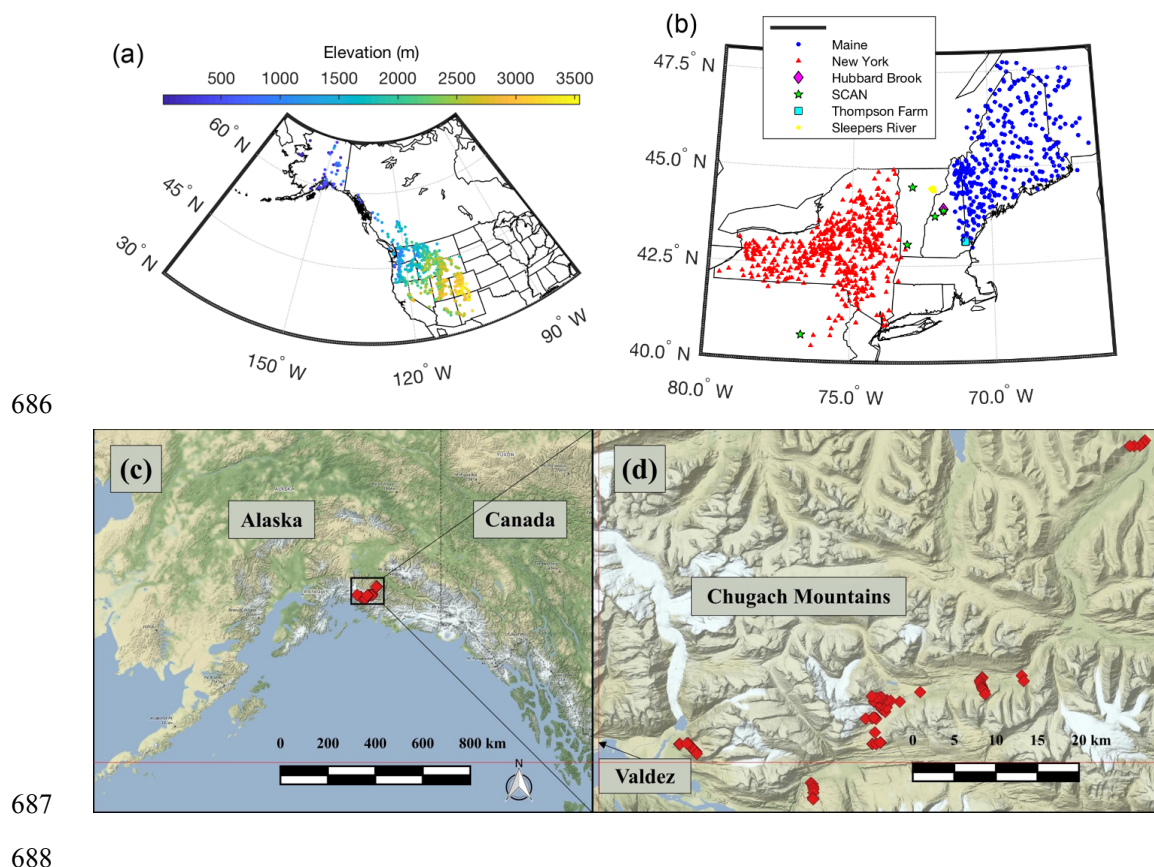
678 Figure 1: Conceptual sketch of the evolution of snow water equivalent (SWE) over the course of a water year (black
679 line). Also shown is the evolution of SWE with snowpack depth over a water year (red line). Note the hysteresis
680 loop due to the densification of the snowpack.



681

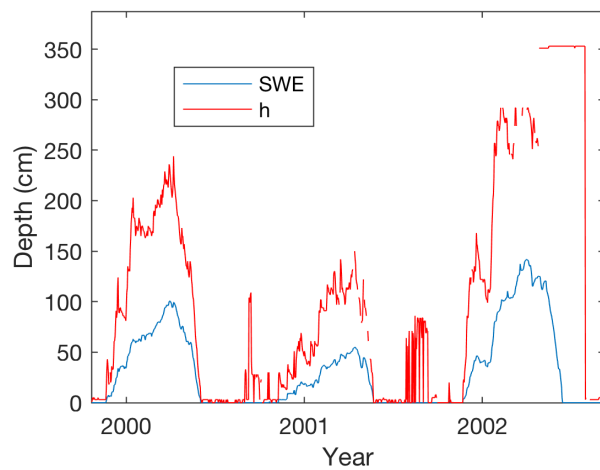


682 Figure 2: Distribution of measurement locations used in this study. (a) Western USA and Canada station locations,
683 with colors indicating station elevation in meters. (b) Northeast USA locations, with stations colored according to
684 data source. (c, d) Measurement sites in the Chugach Mountains, southcentral Alaska.
685





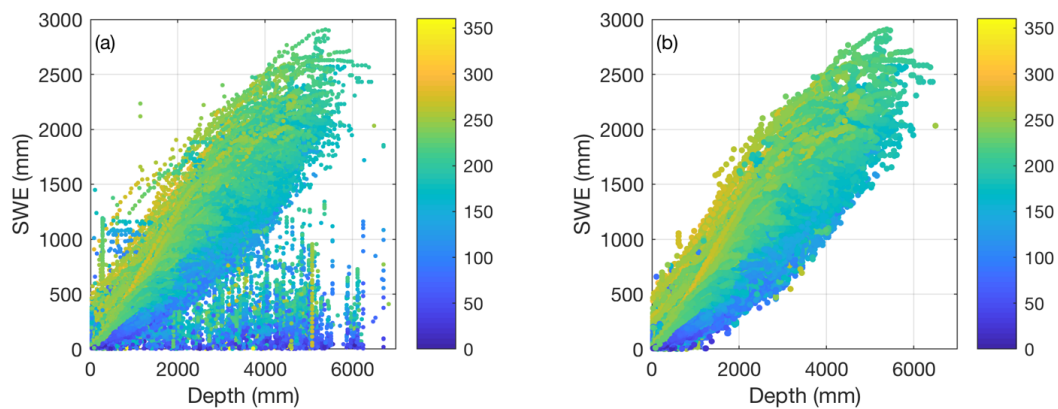
689 Figure 3: Sample time series of SWE and h from the Rex River (WA) SNOTEL station. Observations of h at times
690 when SWE is zero are likely spurious.



691

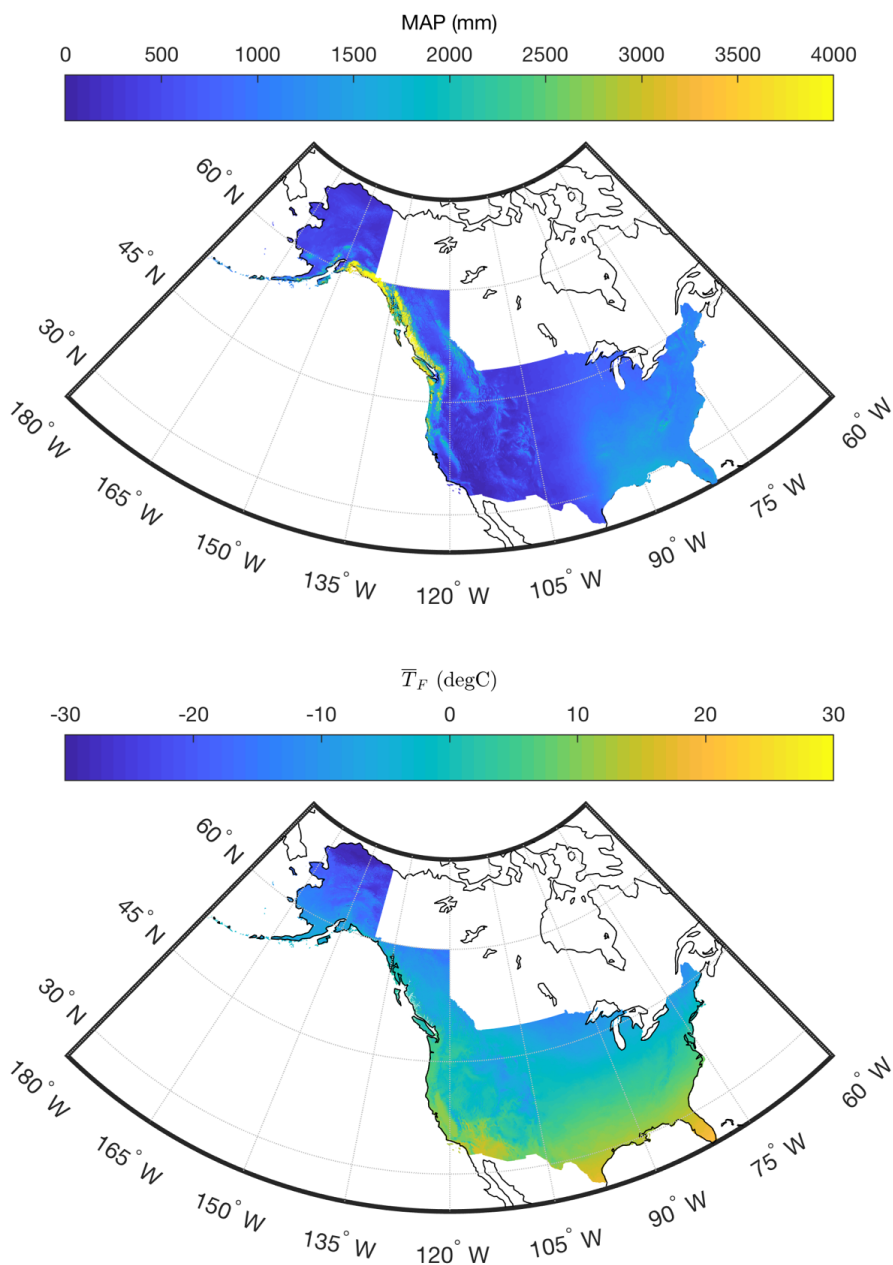


692 Figure 4: Scatter plot of SWE vs. h for the complete SNOTEL dataset before (a) and after (b) removing outliers.
693 Symbols are colored by 'day of water year' (DOY ; October 1 is the origin).
694





696 Figure 5: Gridded maps of mean annual precipitation (MAP) and mean February temperature (\bar{T}_F) for the study
697 regions. Climate normals are from the PRISM data set (1981-2010 for CONUS and British Columbia; 1971-2000
698 for Alaska).

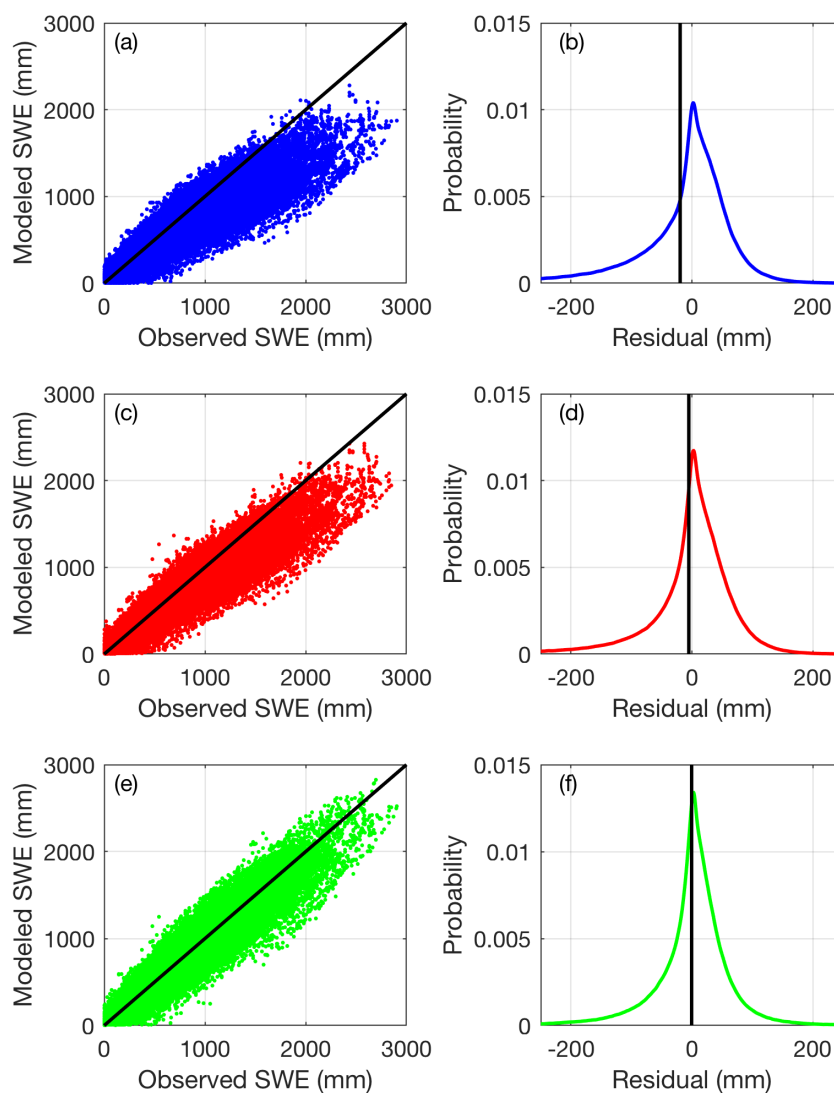


699

700
701



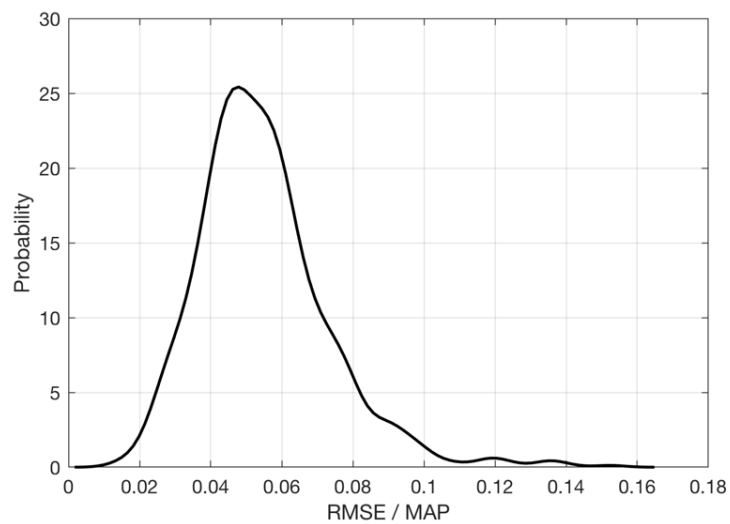
702 Figure 6: Scatter plots (left column) of modeled vs. observed SWE and probability density functions (right column)
703 of the residuals for three simple models applied to the CONUS, AK, and BC snow pillow data. Top row (a-b): One-
704 equation model (Section 2.2.1). Middle row (c-d): Two-equation model (Section 2.2.2). Bottom row (e-f): Multi-
705 variable two-equation model (Section 2.2.3).



706
707



708 Figure 7: Probability density function of snow pillow station root-mean-square error (RMSE) normalized by station
709 mean annual precipitation (MAP).

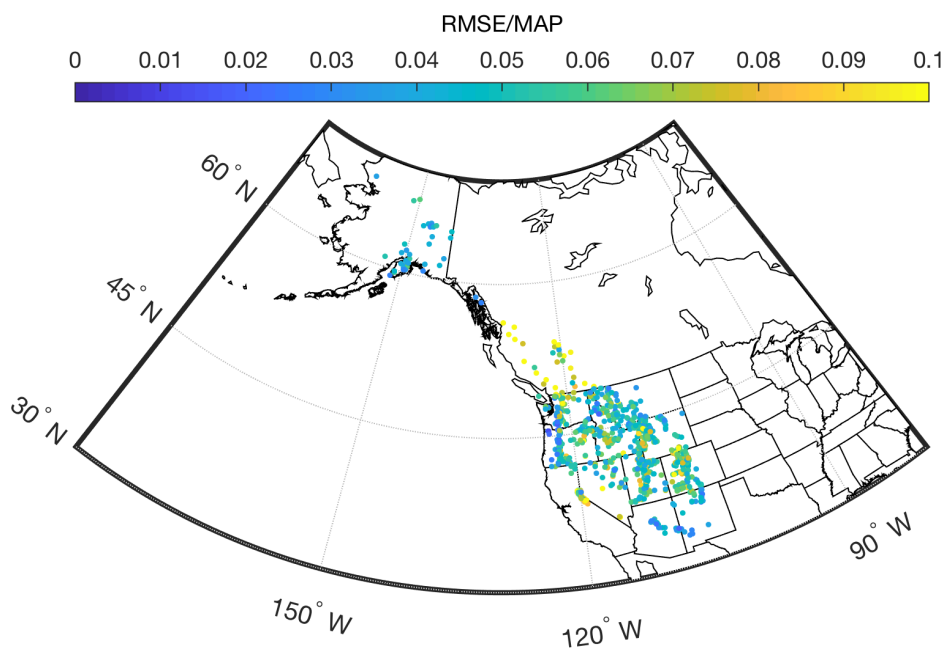


710



711 Figure 8: Spatial distribution of RMSE/MAP at snow pillow stations.

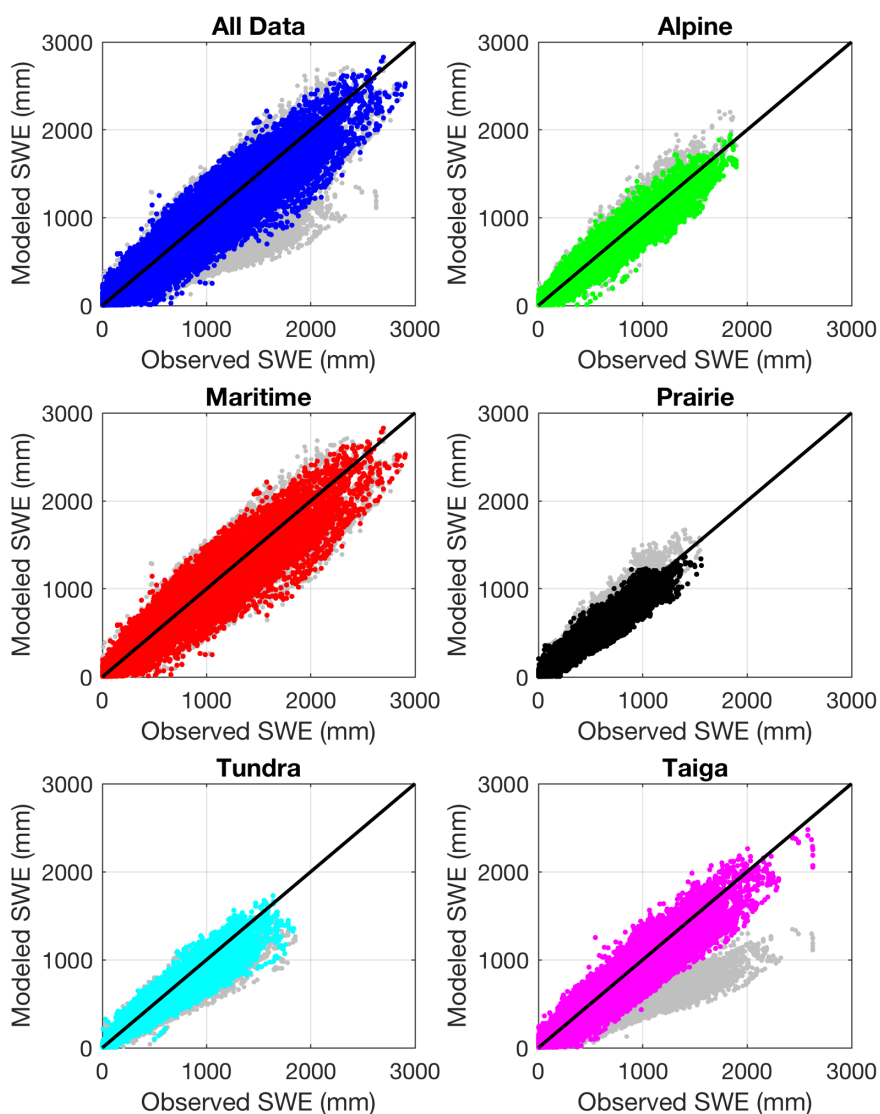
712



713



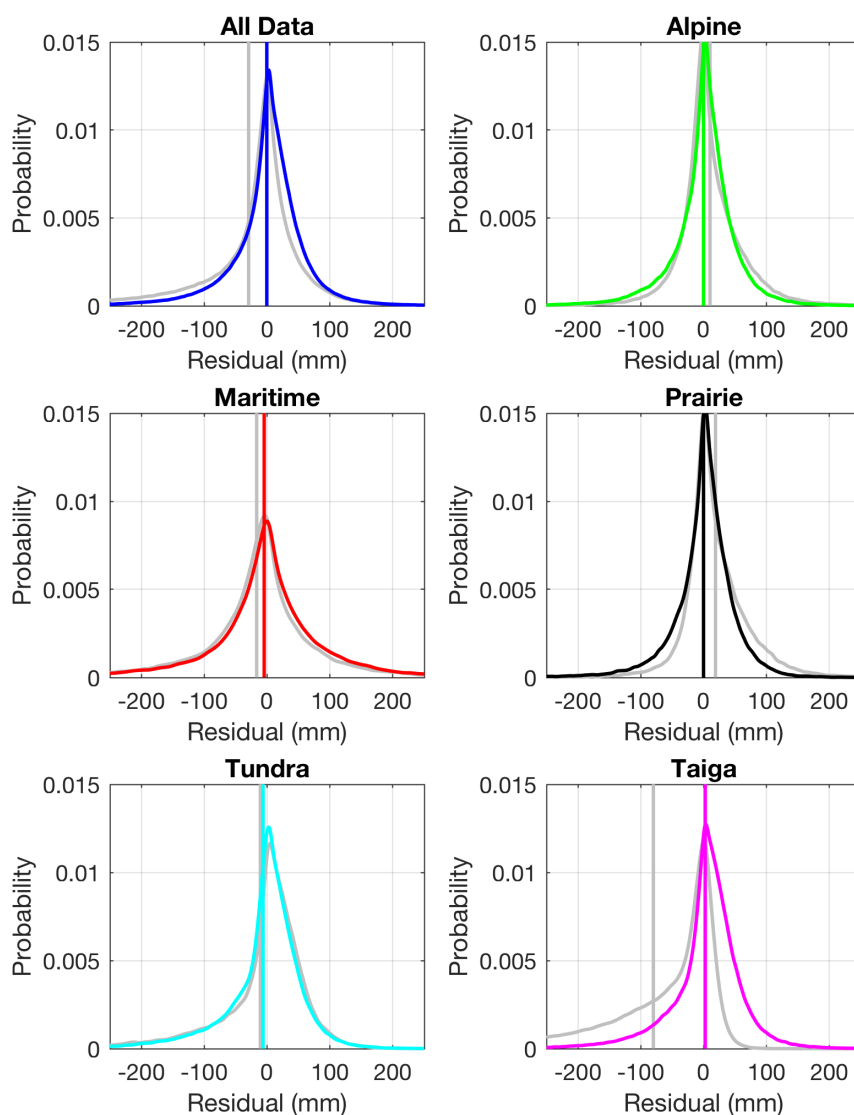
714 Figure 9: Comparison of the multi-variable, two-equation model of the present study with the model of Sturm et al.
715 (2010). The subpanels show modeled SWE vs. observed SWE for all of the data binned together, as well as for the
716 data broken out by the snow classes identified by Sturm et al. (1995). The gray symbols show the Sturm result and
717 the colored symbols (draped on top) show the current result. The models are being applied to the validation data set
718 (50% of the aggregated snow pillow data for CONUS, AK, and BC).



719



720 Figure 10: Comparison of the multi-variable, two-equation model of the present study with the model of Sturm et al.
721 (2010). The subpanels show probability density functions of the residuals of the model fits for all of the data binned
722 together, as well as for the data broken out by the snow classes identified by Sturm et al. (1995). The gray lines
723 show the Sturm result and the colored lines show the current result. The vertical lines show the mean error, or the
724 model bias, for both the Sturm and the current result. The models are being applied to the validation data set (50% of
725 the aggregated snow pillow data for CONUS, AK, and BC).





727 Figure 11: Results from application of the multi-variable, two-equation model to numerous east coast datasets. The
728 left column shows the SWE-*h* data for each dataset. Note that the black symbols are points removed by the outlier
729 detection procedure discussed in section 2.1.1.4. The remaining symbols are colored by DOY. The middle panel
730 plots the model estimates of SWE against the observations of SWE with the 1:1 line included. The right panel shows
731 probability density functions of the model residuals, with the vertical line indicating the mean error, or bias.
732 Individual rows correspond to individual data sets and are labeled.

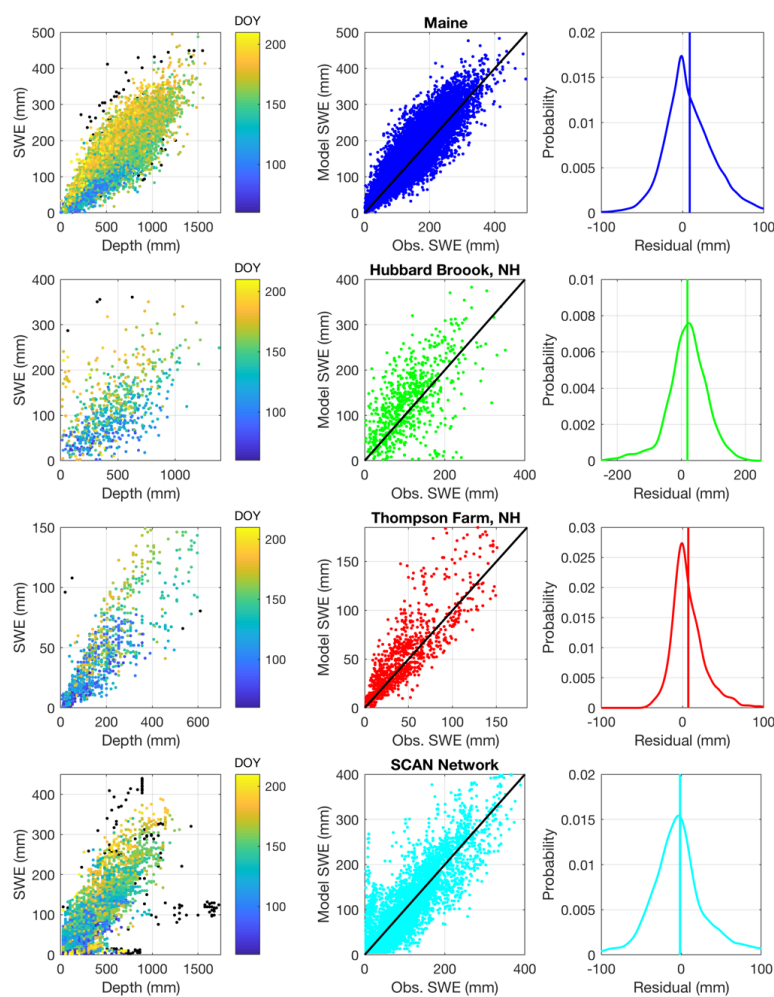
733

734

735

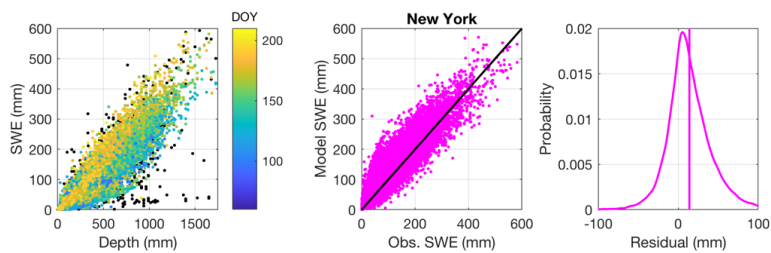
736

737

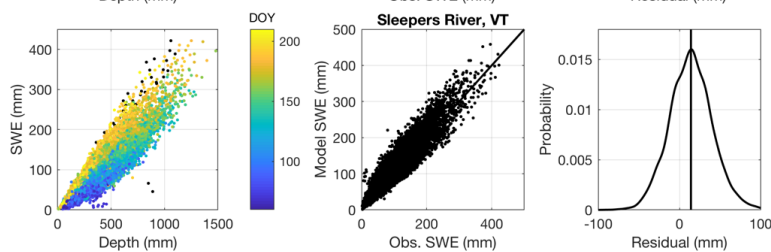




738



739
740





741 Figure 12: Results from application of the multi-variable, two-equation model to the Chugach Mountains, AK. The
742 left column shows the measured SWE-*h* data. The symbols are colored by DOY. The middle panel plots the model
743 estimates of SWE against the observations of SWE with the 1:1 line included. The right panel shows the model
744 residuals, with the vertical line indicating the mean error, or bias.

